Published online 29 September 2008 *Nucleic Acids Research, 2008, Vol. 36, No. 19* ***6187–6198***
doi:10.1093/nar/gkn643

Yeast ribosomal protein L10 helps coordinate tRNA movement through the large subunit

Alexey N. Petrov, Arturas Meskauskas, Sara C. Roshwalb and Jonathan D. Dinman*

Department of Cell Biology and Molecular Genetics, University of Maryland, 2135 Microbiology Building, College Park, MD 20742, USA

Received August 4, 2008; Revised September 16, 2008; Accepted September 17, 2008

ABSTRACT

Yeast ribosomal protein L10 (*E. coli* L16) is located at the center of a topological nexus that connects many functional regions of the large subunit. This essential protein has previously been implicated in processes as diverse as ribosome biogenesis, translational fidelity and mRNA stability. Here, the inability to maintain the yeast Killer virus was used as a proxy for large subunit defects to identify a series of L10 mutants. These mapped to roughly four discrete regions of the protein. A detailed analysis of mutants located in the N-terminal 'hook' of L10, which inserts into the bulge of 25S rRNA helix 89, revealed strong effects on rRNA structure corresponding to the entire path taken by the tRNA 3′ end as it moves through the large subunit during the elongation cycle. The mutant-induced structural changes are wide-ranging, affecting ribosome biogenesis, elongation factor binding, drug resistance/hypersensitivity, translational fidelity and virus maintenance. The importance of L10 as a potential transducer of information through the ribosome, and of a possible role of its N-terminal domain in switching between the pre- and post-translocational states are discussed.

INTRODUCTION

The ribosome is a complex macromolecular machine that orchestrates multiple reactions in a highly coordinated manner. Although atomic level ribosome structures reveal the topologies of the functional centers, how these exchange information and coordinate their activities remains an active field of inquiry. For example, during the translation elongation cycle the ribosome must sequentially bind EF-Tu•aa-tRNA•GTP (ternary complex or TC; in eukaryotes the elongation factor is called 'eEF1A'), stimulate GTP hydrolysis by EF-Tu, accommodate aa-tRNA into the large subunit, effect peptidyltransfer, bind EF-G (eEF2 in eukaryotes), again stimulate GTP hydrolysis by EF-G and translocate along the mRNA by one codon. The TC and EF-G are structurally similar (1), and there is a large degree of overlap between their ribosome binding sites. In yeast, for example, eEF2 contacts the α-sarcin-ricin loop (SRL, H95 of 25S rRNA), the GTPase-associated center (GAC composed of ribosomal protein L12, H43, H44), Helices 33, 34, 69 and 89, ribosomal proteins L9, L12 and the P proteins (P0, P1α, P1β, P2α, P2β) on the large ribosomal subunit, while it also interacts with many elements of the small subunit including h5, h15, h33, h34, h44 in the head and body domains, and with ribosomal protein S23 (2). The interactions between these factors and the ribosome were initially characterized using chemical footprinting methods (3). A cryo-electron microscopy study of the TC stalled on an *Escherichia coli* 70S ribosome with kirromycin revealed a similarly complex set of interactions that included the SRL and the GAC on the large subunit (4).

We have been using a yeast-based system to dissect how the ribosome coordinates TC binding, aa-tRNA accommodation, peptidyltransfer and eEF2 binding. Molecular genetics and biochemical studies using mutant rRNAs and ribosomal proteins are identifying important elements and allosteric rearrangements involved in these processes (5–11). These studies have led us to focus on structural elements in the vicinity of the 'accommodation corridor', a passageway located along the interface between H89 and the H90–H92 structure of the large subunit rRNA (12). Previously, we demonstrated the involvement of a central extension of ribosomal protein L3 in coordinating TC, eEF2 binding and peptidyltransfer by helping to open and close this structure (9).

Ribosomal protein L3 is located on the H90–H92 side of the accommodation corridor. Examination of this

*To whom correspondence should be addressed. Tel: +1 301 405 0918; Fax: +1 301 314 9489; Email: dinman@umd.edu
Present addresses:
Alexey N. Petrov, Department of Structural Biology, Stanford University School of Medicine. D105 Fairchild Science Building, 299 Campus Drive West, Stanford, CA 94305-5126, USA
Sara C. Roshwalb, University of Tennessee College of Veterinary Medicine. 2407 River Dr Knoxville, TN 37996, USA

region reveals that another ribosomal protein, L10 (L16 in *E. coli* and L10e in *Haloarcula marismortui*) is located on the H89 side of the corridor. L10 extends from the solvent accessible side near the factor-binding site down toward the peptidyltransferase center (PTC) in the core of the large subunit. The N-terminal three-quarters of yeast L10 is sandwiched between helices 89 and 38, and appears to be largely structurally conserved with its bacterial and archael homologs (13–16). Inspection of these structures reveals that these proteins represent an extension of H39 of the large subunit rRNA. In cryo-EM reconstitutions, the eukaryote specific C-terminal region of L10 appears to form a large unresolved mass adjacent to the L7/L12 stalk in association with Helix 38 (17). In *Saccharomyces cerevisiae*, L10 is encoded by the essential single copy *RPL10* gene (18). L10 plays a critical role in 60S subunit biogenesis: incorporation of L10 into the large subunit constitutes the last step of 60S subunit biogenesis (19). Specifically, immature large subunits lacking L10 are exported from the nucleus to the cytoplasm via the Crm1p pathway in complex with the export adapter protein Nmd3p, after which L10 is brought to the ribosome in the complex with Sqt1p, promoting release of Nmd3p followed by incorporation of L10. Depletion studies demonstrate that large subunits lacking L10 are unable to form 80S ribosomes and are translationally inactive (20,21). Thus, L10 is the key component required for the final activation step of ribosomes in the cytoplasm. In addition, at least one *rpl10* allele has been shown to inhibit degradation of nonsense-containing mRNAs, suggesting that L10 may play a role in translational fidelity (22). Thus, L10 is important both for ribosome assembly and post-transcriptional regulatory processes.

Toward the goal of furthering our understanding of L10, a primary library of randomly mutagenized *rpl10* alleles was screened for the inability to maintain the yeast 'Killer' phenotype, which is caused by an endogenous dsRNA virus that is highly sensitive to a broad array of changes in the translational apparatus (23). This forward genetic screen identified 56 new *rpl10* alleles. The mutants generally clustered into four regions of the L10 structure: (i) in a 'hook' of L10 that inserts into the bulge at the base Helix 89; (ii) in a cluster that appears to form a bridge between Helices 38 and 39; (iii) a series of amino acids that appear to form a plane along the face of L10 that interacts with the distal regions of Helices 89 and 38; and (iv) amino acids present in the unresolved region of the protein that may directly interact with the GTPase-associated center. The current study focuses on the N-terminal 'hook' region of L10. A series of genetic and biochemical studies led to a detailed analysis of the effects of two mutants in this region on 25S rRNA structure. These were found to promote structural changes that map along the path taken by tRNAs through the elongation cycle. When considered along with the physical location of L10 within the large subunit and its role in ribosome biogenesis, the finding presented here are used to build a model for how L10 plays an important role for coordinating tRNA passage through the ribosome.

MATERIALS AND METHODS

Strains, media and genetic methods

Escherichia coli strain DH5α was used to amplify plasmids, and *E. coli* transformations were performed using the high-efficiency transformation method (24). The haploid *S. cerevisiae rpl10* gene deletion strain AJY1437 (*MATa met15Δ0 leu2Δ0 ura3Δ0 his3Δ0 RPL10::kan*^{R} pAJ392) was a kind gift from Dr. A.W. Johnson. The L-A and M_1 dsRNA viruses were introduced into this strain by cytoplasmic mixing (cytoduction) (25) using strain JD759 [*MATα kar1-1 arg1 thr(i,x)* (L-A HN M_1)] as the cytoplasm donor. The resulting strain was designated JD1293 [*MATa rpl10::Kan met15Δ0 leu2Δ0 ura3Δ0 his3Δ0* p*RPL10-URA3*-2μ (L-A HN M_1)]. Yeast cells were transformed using the alkali cation method (26). YPAD and synthetic complete medium (H-), as well as YPG, SD and 4.7 MB plates used for testing the killer phenotype were prepared and used as described previously (27). Oligonucleotide primers were purchased from IDT (Coralville, IA). Dual luciferase assays to quantitatively monitor translational recoding in yeast were performed as previously described (28). The latter involved use of a 0-frame control reporter in combination with −1 ribosomal frameshift, or nonsense suppression test reporter constructs. Recoding efficiencies and statistical analyses were performed as previously described (28,29). Ten-fold dilution spot assays to monitor sensitivity to anisomycin (20 μg/ml) or paromomycin (3 mg/ml) were performed as previously described (30).

Generation of *rpl10* alleles

A library of plasmid-borne *rpl10* mutants was constructed using the error-prone PCR and gap repair method (31) based on pJD589. To create pJD589, a 1-kb fragment containing the 5′ promoter, open reading frame and 3′ untranslated region (UTR) sequences of *RPL10* was subcloned from the *URA3-2μ* vector pAJ392 into the BamHI sites of pRS313 (32). Silent mutations were added into codons 4, 5, 220 and 221 of the *RPL10* ORF to create two StuI restriction sites. Mutagenesis primers (70 nt) for PCR were designed to be complementary to the 5′ and 3′ UTRs of *RPL10* and include the *RPL10* translational start and stop codons: (forward 5′TTCCGCAAGTGC TTTTGGAGTGGGACTTTCAAACTTTAAAGTACA GTATATCAAATAACTAATTCAAGATGGCTAGAA GG3′, reverse 5′AATTACTGTTTAATAAACTAGAAT TTAAATCAAAAAAATTTCTCTTTTAAGTTAGTTC AAATGTTTGAAAAGAACTTAGG3′). Random mutagenesis was performed with the GeneMorph II PCR random mutagenesis kit with template concentrations optimized to generate between one and four mutations per *RPL10* coding sequence. pJD589 was digested with StuI, and the linearized plasmid lacking the *RPL10* coding sequence was purified by Tris–acetate–EDTA–agarose gel electrophoresis. This was cotransformed with the randomly PCR-mutagenized *RPL10* coding sequences into JD1293 cells. Recombinants were selected for growth on medium lacking histidine (-his), and cells having lost the wild-type *RPL10*-containing plasmids were selected

for by replica plating onto 5-fluoroorotic acid (5-FOA)-containing medium (33). Note that recombination between the PCR product and linearized vector was designed so that the silent mutations would revert to wild-type sequence in the recombinant clones.

Identification of *rpl10* alleles unable to support the yeast killer virus

Approximately 3000 His^+ colonies were arrayed onto -his plates, replica plated onto 4.7 MB plates seeded with 5×47 killer indicator cells, and incubated at 20°C to identify $Killer^-$ (K^-) colonies as previously described (34). Plasmids harboring *rpl10* alleles were rescued into *E. coli* from yeast strains that had lost the killer phenotype, reintroduced into JD1238 cells and rescored for the inability to maintain the killer phenotype. The procedure was performed three times in order to prevent identification of false positive strains due to spontaneous Killer virus loss.

RNA blot analyses

RNA (northern) blotting was performed as previously described (35). Total RNA was extracted with acid phenol/chlorophorm (pH = 4.5) from mid-logarithmic cell cultures as previously described (36). Equal amounts of RNA (2.5 μg) were separated through a 1% agarose-formaldehyde gel, RNA was transferred to a Hybond-N membrane (Amersham) and UV cross linked to the membrane. Nonspecific binding sites on the membrane were blocked using ULTRAhyb-Oligo buffer (Ambion), incubated with a [^{32}P] 5′-end-labeled oligonucleotide (5′C CGGGGTGCTTTCTGTGCTTACCGATACGACCTT TACCGGCTG3′) complementary to the 5′ end of the CYH2 CDS, and subsequently washed according to manufacturer's instructions. Hybridizing species were identified using a GeneStorm phosphoimager (Bio-Rad), and quantified using QuantifyOne software from Bio-Rad.

Ribosome biochemistry and visualization

Lysates of cycloheximide arrested yeast cells were sedimented through 7–47% sucrose gradients and polysome profiles were determined by monitoring A_{254} nm as previously described (37). *S. cerevisiae* ribosomes were isolated, yeast aminoacyl-tRNA synthetases were purified and yeast phenylalanyl-tRNAs were aminoacylated with [^{14}C]Phe and purified by HPLC as previously described (6). Single-round peptidyltransfer assays using Ac-[^{14}C]Phe-tRNA and puromycin, and equilibrium binding studies of [^{14}C]Phe-tRNA binding to the ribosomal A-site were carried out using poly(U) primed ribosomes as previously described (6). Equilibrium binding studies of eEF-2 were performed as previously described (9). The data were fitted to a one-site-binding model with ligand depletion using Prism Graph Pad software. rRNA structure analysis using DMS, kethoxal and CMCT were performed as previously described (9). The X-ray crystal structure of the *H. marismortui* 50S ribosomal subunit (1VQ6) (38), the cryo-electron microscopy (cryo-EM) reconstruction of *S. cerevisiae* ribosomal proteins threaded onto the X-ray crystal structure of the *H. marismortui* 50S ribosomal subunit (PDB IS1I) (2), the *Thermus thermophilus* 70S ribosome complexed with two tRNAs at 2.8 Å resolution (PDB 2J00 and 2J01) (14), the *T. thermophilus* 70S ribosome complexed with a model mRNA and two tRNAs at 3.7 Å resolution (PDB 2I1C and 1VSA) (15), the *E. coli* ribosome complexed with three tRNAs at 3.5 Å (2AW4) (13), the *T. thermophilus* 70S ribosome with a model mRNA and tRNAs at 5.5 Å (2HGU) (39) and a cryo-EM reconstruction of the D. radiodurans ribosome complexed with thiostrepton at 3.3–3.7 Å (2ZJR) (40) were visualized using PyMOL (DeLano Scientific LLC).

RESULTS

Identification of translationally defective *rpl10* alleles

Prior studies have implicated L10 with a broad range of ribosome-associated functions, including large subunit maturation, subunit association and NMD. These facts, in combination with the centralized location of L10 within the 3-D structure of the large subunit, provided us with the motive to pursue an in-depth molecular genetic and biochemical analysis of L10 function. Toward to this end, a library of randomly mutagenized *rpl10* alleles was screened for the inability to maintain the yeast killer phenotype. The killer system of yeast is composed of L-A helper, and M_1 satellite dsRNA viruses (41). The genome of the L-A virus encodes two open reading frames where the first encodes the *Gag* (capsid) protein, and the second encodes a viral RNA-dependent RNA polymerase (RDRP), the production of which is dependent on a programmed –1 ribosomal frameshift (–1 PRF) (42,43). The single open reading frame of the M_1 satellite virus encodes a protein toxin that is exported into the surrounding media and kills uninfected cells, thus producing the easily detectable $Killer^+$ (K^+) phenotype, and its maintenance requires L-A to supply capsid proteins and RDRP. M_1 is highly sensitive to small perturbations in the translational apparatus, including changes in –1 PRF efficiency (34), ribosome biogenesis defects (44) and decreased overall protein synthesis (45). Thus, the killer assay provides a simple and rapid method to screen for translational defects.

The coding region of *RPL10* was subjected to random PCR mutagenesis and screened for loss of the killer phenotype as described in the Materials and methods section. Mutant *rpl10-HIS3* plasmids were rescued from Killer minus (K^-) strains, passaged through *E. coli*, reintroduced into *rpl10Δ* cells and rescored for their abilities to promote M_1 virus loss. Due to a significantly high intrinsic rate of killer loss in the JD1293 strain background (~10%), the plasmid rescue and reintroduction procedure was repeated three times to eliminate false-positive results. The *rpl10* mutations responsible for conferring the K^- phenotype were identified by DNA sequence analysis. From >3000 colonies tested, a total of 56 unique mutants were identified. In addition, ~15% of the mutants were lethal as determined by their inability to grow as the sole allele of *rpl10* (data not shown). The collection of K^- mutants contained alleles harboring 35 single mutations, 20 double mutations and one triple mutant. These are summarized in Supplementary Table 1. A very large amount of overlap

was observed between the single and double mutants. The high degree of overlap between the single and double mutants led us to conclude that the mutagenesis was performed to near saturation, and the large number of alleles with single amino acid substitutions allowed exclusion of alleles with multiple mutations from subsequent analysis. Among the single mutants, multiple substitutions were found at amino acid residues 7, 9, 40, 93, 94 and 145. Areas of L10 with high frequencies of mutations were clustered in three regions of the protein. These regions spanned amino acids 7–17, 59–94 and 144–152. Consistent with findings from the Johnson lab, no viable mutants mapping to the unstructured central loop (amino acids 102–112) were identified in the current study, consistent with the suggestion that his loop may play a critical function in peptidyltransfer (46). As diagramed in Figure 1, the mutants appear to cluster into four distinct groups, specifically: (i) in a hook-like structure located at the N-terminal region of L10 that inserts into the major groove of helix 89; (ii) in a space that appears to link helices 38 and 39; (iii) along a plane of the protein lying 'atop' of helix 89; and (iv) in the unresolved C-terminal domain of L10 that appears to extend outward toward the GTPase-associated center. Given this apparent structural complexity of L10, we chose to focus on characterizing the N-terminal 'hook domain' mutants for this study.

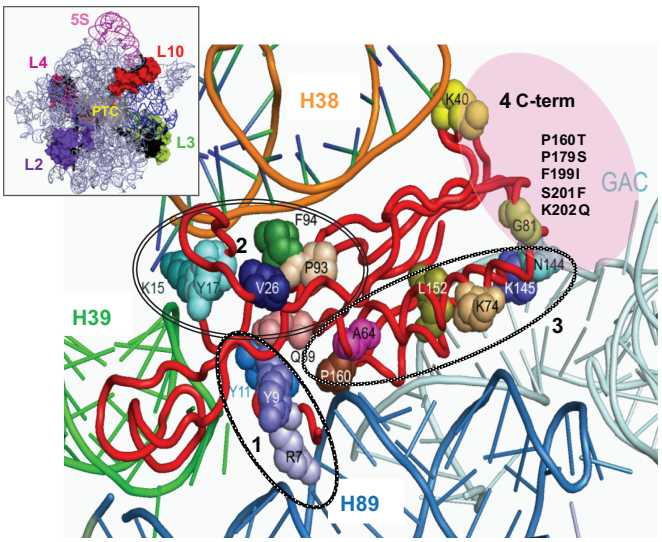

Figure 1. Localization of the L10 mutations identified in this study. Insert shows the 'crown view', and the general location of L10 relative to other salient features of the large subunit. Large picture shows the L10 mutants mapped onto the structure of yeast L10 taken from (2). The four spatially defined groups of L10 mutants are circled and labeled, where group 1 represents those located at the N-terminus of the protein. Group 4, indicated by the pink circle, map to the structurally undefined C-terminal region of yeast L10. Neighboring 25S rRNA helical structures are indicated, and GAC indicates the GTPase-associated center of the large subunit.

The N-terminal 'hook' mutants affect cell growth

Ribosome-associated defects commonly promote deficiencies in cellular growth at ambient temperature. As a semi-quantitative monitor of this, 10-fold dilution spot assays were performed on rich medium at 30°C, revealing allele-specific growth defects by the R7Q and Y11C mutants (Figure 2A). Note that the large colonies in the Y11C sample appear to be escape mutants. Changes in ribosome structure and function also alter the growth characteristics of cells at decreased and/or elevated temperatures. Thus, these mutants were assayed with regard to their resistance or sensitivity to low (15°C) and high (37°C) temperatures. As shown in Figure 2B, mutations of the tyrosines in the N-terminal region of the protein bridging helices 89 and 39, i.e. Y9H, Y9N and Y11C promoted enhanced growth at low temperature. In contrast, none of these mutants affected growth at 37°C (Figure 2C). Ten-fold serial dilution assays were also used to probe the effects of small molecule protein synthesis inhibitors on the translational apparatus. Anisomycin is a competitive inhibitor of A-site binding and sterically hinders positioning of the acceptor end of the A-site tRNA in the PTC (47). All of the other mutants were either hypersensitive as determined by reduced growth at 15 μg/ml anisomycin (R7Q, Y9H, Y9N and Y11C), or resistant as evidenced by the ability to grow on medium containing 20 μg/ml anisomycin (R7L, R7P and Y9C) (Figure 2D and E, and summarized in Table 1). These data indicate a high degree of allele-specificity with regard to this drug. Another small molecule drug, paromomycin, binds at the decoding center on the small subunit and promotes conformational changes associated with formation of the codon–anticodon helix between mRNA and incoming A-site tRNA (48). Thus, paromomycin was used as a probe for defects associated with interactions between the small and large subunits.

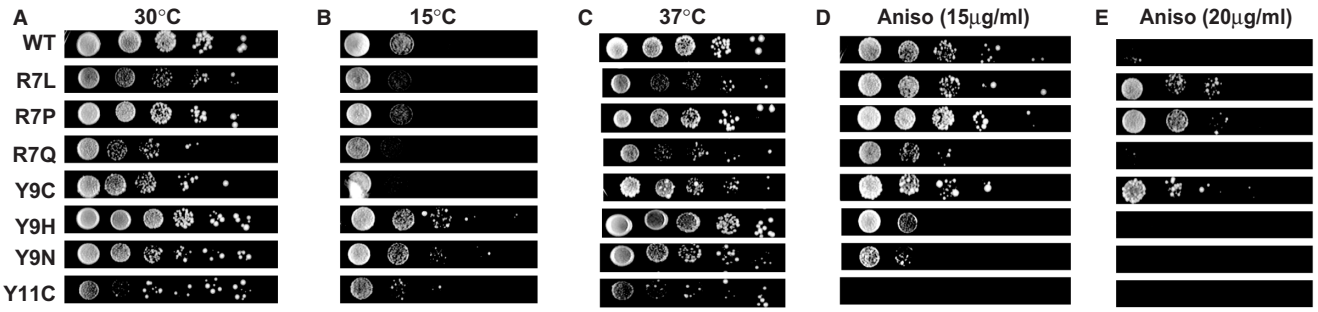

Figure 2. Genetic phenotypes of the L10 N-terminal hook mutants. Ten-fold dilutions of cells harboring the indicated *rpl10* alleles were spotted onto complete synthetic medium lacking histidine (-his), and were incubated at the indicated temperatures (three left panels). In the two right panels, cells were spotted onto -his medium containing the indicated concentrations of anisomycin.

None of the mutants promoted paromomycin-specific changes in growth (data not shown), thus indicating that the observed effects on cell growth were conferred by changes in the large subunit.

Effects on translational fidelity

Alterations in ribosome structure can affect the fidelity of protein translation. Changes in –1 PRF have been shown to interfere with virus propagation by altering the ratio viral Gag to Gag-pol proteins (34), and thus altered –1 PRF frequencies could be one possible reason underlying the K^- phenotypes of the *rpl10* mutants. An *in vivo* dual-luciferase reporter assay and statistical analysis package (28,29) was used to quantitatively assess –1 PRF in the wild-type *RPL10*, and isogenic *rpl10* strains. In wild-type cells, –1PRF was 8.3 ± 0.16%. Surprisingly, –1PRF efficiency was not strongly affected in any of the *rpl10* mutant strains (Figure 3A, white bars) suggesting that –1 PRF defects were not the major cause of the K^- phenotypes. The dual luciferase assay was also used to quantitatively access the effects of the *rpl10* alleles on the ability of ribosomes to recognize termination codons (nonsense suppression). This analysis revealed strong allele-specific effects (Figure 3A, gray bars). While nonsense suppression was 0.27% ± 0.01% in wild-type cells, it was stimulated by ~1.5-fold by the R7L mutant but not by the other two mutants as this position. In contrast all of the Y9 mutants appeared to promote hyperaccurate termination codon recognition, decreasing rates of nonsense-suppression by 1.8-fold (Y9C) and 2.5-fold (Y9N). The translational fidelity data are summarized in Table 1.

It had been previously shown that the *grc5-1* allele of *RPL10* promoted defective turnover of nonsense-containing mRNAs (22). Although the bicistronic reporters internally control for apparent changes in translational fidelity due to effects on mRNA stability (28,49), to further exclude this possibility and to determine whether any of the new *rpl10* alleles affected nonsense-mediated mRNA decay, levels of the inefficiently spliced CYH2 precursor-mRNA were assayed by northern blot analysis using total RNA extracted from cells expressing the three *rpl10* alleles that most affected nonsense-suppression, and from control isogenic wild-type and *upf1Δ* cells. While the CYH2 pre-mRNA was stabilized in the *upf1Δ* strain, none of the mutants appeared to stabilize this species relative to isogenic wild-type controls (Figure 3B), confirming their effects on nonsense-suppression.

All of the L10 N-terminal hook mutants affect 60S subunit biogenesis

L10 is the last protein incorporated into the large subunit and is required for formation of active ribosomes (50). During translation initiation, the 43S complex recruits the mRNA to form the 48S complex, after which the 60S subunit is recruited. Insufficient levels of 60S subunits, or 60S subunits deficient in their ability to form 80S ribosomes, tend to promote accumulation of 48S–mRNA complexes, and this additional mass results in intermediate sedimentation coefficients as monitored by the appearance of 'halfmers shoulders' on the denser sides of polysome tracings. L10 mutants affecting inclusion of the protein into large subunits have been shown to promote the appearance of these halfmer shoulders in polysome profiles (21), and 60S ribosomal subunit biogenesis defects have been linked with defects in killer virus maintenance (44). Sucrose gradient analyses revealed that all but the Y9H and Y11C mutants promoted formation of halfmers (Figure 3C), many with greater amplitude than previously observed in the temperature sensitive mutants (21). Additionally, observation of decreased amplitude of the 60S relative to 40S peaks, of 80S relative to 40S and 60S peaks, or an increase in the amount of material near the top of the gradient are also associated with 60S subunit biogenesis defects. These effects were observed in the R7L, R7Q, Y9C, Y9H, Y9N and Y11C mutants (summarized in Table 1). These results point to 60S subunit ribosome biogenesis defects as the most likely cause of the inability of the *rpl10* mutants to maintain the killer virus.

Table 1. Summary of the L10 N-terminal 'hook' mutants examined in this study

Strain	Percentage of −1PRF (fold-WT)[a]	Nons. Supp. (fold-WT)[b]	Aniso[c]	aa-tRNA K_d, nM (fold-WT)[d]	eEF2 K_d, nM (fold-WT)[e]	Ribo biogenesis defects[f]
WT	8.30 ± 0.16	0.27 ± 0.01		86 ± 9	10.8 ± 1.6	No
R7L	7.71 ± 0.69 (0.93)	0.40 ± 0.05 (1.50)	Resistant	114 ± 8 (1.32)	10.7 ± 1.8 (0.99)	Yes
R7P	7.42 ± 0.39 (0.89)	0.30 ± 0.02 (1.11)	Resistant	153 ± 7 (1.78)	6.6 ± 1.6 (0.61)	Yes
R7Q	8.21 ± 0.57 (0.99)	0.26 ± 0.02 (0.98)	Wild-type	198 ± 71 (2.30)	6.1 ± 1.6 (0.56)	Yes
Y9C	11.18 ± 0.34 (1.35)	0.11 ± 0.04 (0.40)	Resistant	690 ± 147 (8.02)	5.2 ± 1.2 (0.48)	Yes
Y9H	10.69 ± 0.37 (1.29)	0.19 ± 0.07 (0.71)	Sensitive	142 ± 16 (1.65)	9.0 ± 1.9 (0.84)	No
Y9N	9.12 ± 0.31 (1.10)	0.15 ± 0.08 (0.56)	Sensitive	154 ± 9 (1.79)	9.7 ± 1.7 (0.9)	Yes
Y11C	11.59 ± 0.88 (1.40)	0.32 ± 0.04 (1.19)	Hyper-sens	74 ± 11 (0.86)	16.6 ± 1.2 (1.54)	Yes

± Denotes standard errors throughout.
[a]Efficiency of −1 ribosomal frameshifting. Numbers in parentheses denote fold wild-type levels throughout.
[b]Percent rate of suppression of an in-frame UAA codon.
[c]Resistance or hypersensitivity to anisomycin relative to wild-type.
[d]Dissociation constants of ribosomes for the aa-tRNA•eEF1A•GTP Ternary Complex (nM).
[e]Dissociation constants of ribosomes for eEF2 (nM).
[f]Indicates the effects of the indicated L10 mutants on ribosome biogenesis/subunit joining.

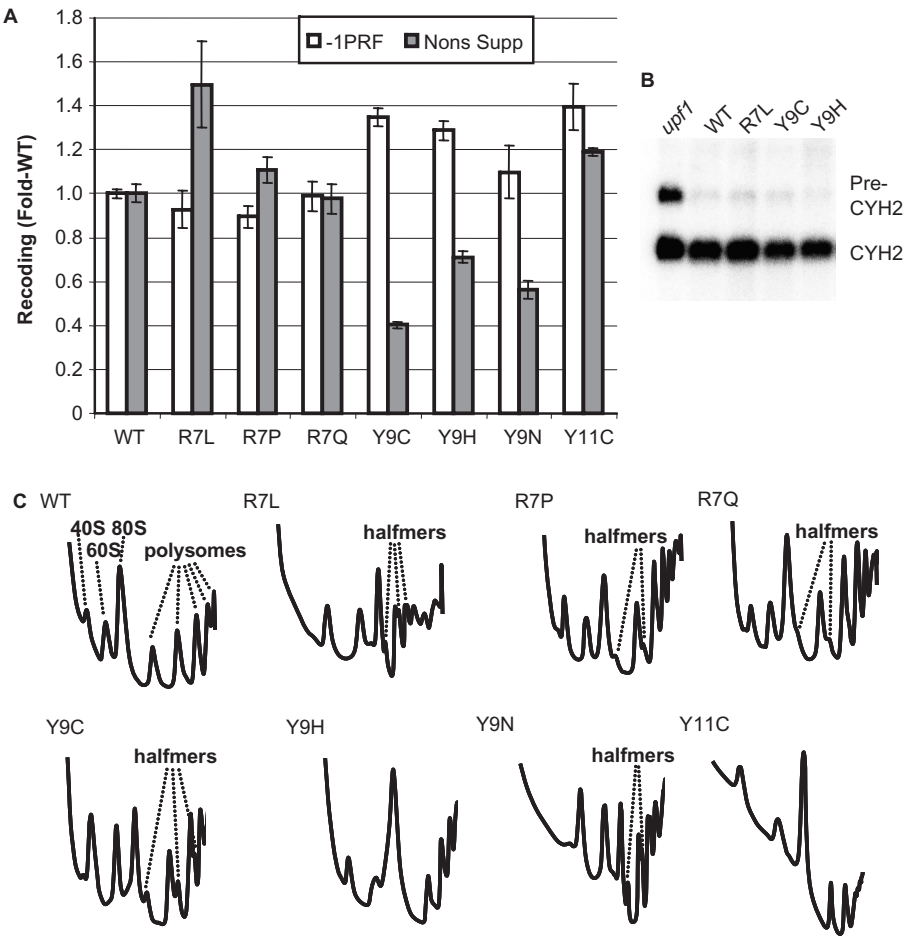

Figure 3. The L10 N-terminal hook mutants promote allele-specific effects on nonsense codon recognition and ribosome biogenesis/subunit joining. (**A**) Allele-specific effects on nonsense codon recognition but not programmed –1 ribosomal frameshifting (–1 PRF). Isogenic yeast cells expressing either wild-type or mutant forms of L10 were transformed with dual luciferase reporter and control plasmids (28) and rates of translational recoding were determined. –1 PRF indicates programmed –1 ribosomal frameshifting promoted by the yeast L-A virus frameshift signal. Nons-supp. denotes the ability of ribosomes able to suppress an in-frame UAA termination codon located between the *Renilla* and firefly luciferase reporter genes. Relative differences in recoding efficiencies of the mutants is depicted as fold of wild-type. Error bars denote standard error as previously described (29). (**B**) The mutants do not affect nonsense-mediated mRNA decay. A northern blot of total RNA extracted from isogenic wild-type and indicated L10 mutants was probed with a [^{32}P]-labeled synthetic oligonucleotide complementary to the yeast CYH2 coding sequence as previously described (62). Locations of the unspliced CYH2 pre-mRNA and of the mature CYH2 mRNA are indicated. (**C**) Most of the L10 mutants promote strong 60S biogenesis and subunit joining defects. Cytoplasmic extracts from isogenic strains were loaded onto 7–47% sucrose gradients, centrifuged in an SW41 rotor at 40 000 r.p.m. for 180 min at 4°C, fractionated and analyzed by continuous monitoring of A_{254} (63). The locations of 40S, 60S, 80S, polysome fractions and halfmers are labeled. The presence of halfmers is typically due to subunit joining defects or to lower abundance of 60S subunits as a consequence of 60S biogenesis defects.

Ribosome biochemistry

Previous studies from our laboratory using mutants of ribosomal protein L3 demonstrated an inverse relationship between the affinity of ribosomes for aa-tRNA and eEF2 (9). Equilibrium dissociation constants were determined for aa-tRNA using of [^{14}C]Phe-tRNA and non-salt-washed ribosomes, and for eEF2 by monitoring the ability of diphtheria toxin to label ribosome bound eEF2 with [^{14}C]NAD^{+}. The inverse relationship between aa-tRNA and eEF2 affinities was also observed with the L10 mutants (Figure 4, Table 1 and Supplementary Figure 1). In all cases, increased affinity for aa-tRNA was matched by decreased affinity for eEF2 and *vice versa*. In particular, the Y9C and Y11C mutants showed dramatically opposing effects on these two parameters. The Y9C mutant promoted an ~8-fold increase in K_d for aa-tRNA, and an ~50% decrease in Kd for eEF2. Conversely, the K_ds of Y11C ribosomes for aa-tRNA were 0.86- and 1.54-fold of wild-type. No significant changes in peptidyltransferase activities were observed between wild-type and mutant ribosomes (data not shown).

Chemical protection studies: the Y9C and Y11C forms of L10 produce profound local and long-distance changes in 25S rRNA structure

In light of their strong and opposing effects on aa-tRNA and eEF2 binding, the effects of the Y9C and Y11C mutants on 25S rRNA structure were probed using three

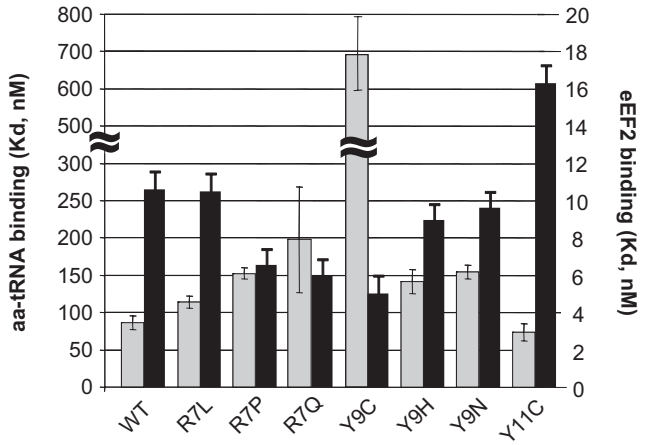

Figure 4. An inverse relationship between ribosome binding with the aa-tRNA and eEF2. Dissociation constants were generated by analysis of single-site-binding isotherms of eEF-1A stimulated binding of [^{14}C]Phe-tRNA to ribosomal A-sites in the presence of GTP (aa-tRNA, gray bars), or with eEF2 (black bars) as determined by monitoring the fraction of [^{14}C]-ADP-ribosylation of ribosome associated eEF2 by diphtheria toxin. Error bars denote standard deviation. The equilibrium binding curves from which these data were generated are shown in Supplementary Figure 1.

base-specific solvent-accessible reagents: dimethylsulfate (DMS), kethoxal and carbodiimide metho-*p*-toluenesulfonate (CMCT). rRNAs were extracted, and modified bases were identified by primer extension using reverse transcriptase to detect methylation at the N3 position of uridines and the N1 position of guanosines (CMCT), at the N1 and N2 positions of guanosines (kethoxal), and at the N1 position of adenosines and N3 position of cytidines (DMS) (51). The primers used were designed to probe functional regions of domain V (including the A-site and P-site loops, the PTC, and the helices adjacent to these structures, i.e. Helices 73, 74, 88–93), Helices 94–96 and Helix 38 (9,11).

Autoradiograms generated from these experiments are shown in Figure 5A. Figure 5B and C show 2-dimensional maps of the relevant regions of yeast 25S rRNA onto which nucleotides having altered chemical protection patterns in the Y11C and Y9C mutants have been mapped. This information was in turn used to map the modified bases onto the structure of the yeast ribosome (2) in Figure 5D and E. The chemical protection patterns are also mapped onto five additional high-resolution ribosome structures (Supplementary Figure 2). Although no significant differences were observed in the locations of bases with chemical modification changes, as discussed below, this analysis did reveal differences in the locations of the N-terminal hook domain. Examination of the data reveals that both of the mutants confer significant changes in 25S rRNA structure. The Y11C mutant is marked by significant changes radiating outward and parallel to L10 from the site of the mutation along Helices 89 and 38 (and expansion segment 12, which is not present in the atomic resolution structure) (Figure 5A, B and D). The affected bases in these structures are mostly deprotected, suggesting that the Y11C mutant destabilizes interactions between L10 and these rRNA helical structures. Interestingly, the changes in H38 and H89 are similar to those promoted by rRNA mutants located in Helix 38 (7). An additional series of long-distance changes are observed extending along a line from the base of the peptidyltransferase center (G2813–G2815) along Helix 74 and out to Helix 88: as discussed below, this follows the path taken by the 3′ end of the deacylated tRNA as it moves from the P-site to the E-site and exits the ribosome. The affected bases in this cluster tend to be hyperprotected as compared to wild-type ribosomes, suggesting that the Y11C promoted disruption of the local interactions between L10 and Helices 38 and 89 has caused them to collapse into more distantly located structures. This pattern is also similar to one observed by another rRNA mutant, Ψ2922C, located at the base of Helix 92 in the A-loop (11). Additionally, one base at the tip of Helix 91 (A2901, *E. coli* U2583), which abuts the SRL, became hyperprotected by this mutant. Attention is directed to four specific bases. First, U2860 (*E. coli* U2483) helps to form one side of the first 'gate' through which aa-tRNA passes during the process of accommodation (12). Second, A2818 (*E. coli* A2450) is located in the core of the peptidyltransferase center. Third, G2815 (*E. coli* G2447) was hyperprotected by this mutant and is discussed in the context of anisomycin hypersensitivity. Fourth, G2777 (*E. coli* A2406) which is normally base-paired with C311 (*E. coli* U416) in helix 22 became deprotected, and C2775 (*E. coli* U2404) displayed an enhanced in-line cleavage pattern, suggesting an opening of a proposed E-site gate responsible for movement of tRNA from the P-site to the E-site and release of deacylated tRNA from the ribosome.

Examination of the effects of the Y9C mutant on 25S rRNA chemical protection patterns reveals a distinctly different picture marked by more local changes along the aa-tRNA accommodation corridor (Figure. 5A, C and E). Proximal to the mutant amino acid, U2828 (*E. coli* U2460) was hyperprotected, suggesting that an interaction between it and L10 were significantly altered. Deprotection of bases in Helix 38 (A1947, A1048) and Helix 89 (A2844, A2850) that appear to interact with other parts of L10 suggests that the local change may have radiated outward from the mutated residue disrupting the interaction of L10 with these helices. Hyperprotection of bases along the aa-tRNA accommodation corridor, in particular U2861 (*E. coli* U2492) and U2923 (*E. coli* U2555), and extending outward to regions of Helix 95, suggests collapse of this structure into the corridor. Finally, the strong deprotection of A2818 and A2819 (*E. coli* A2450 and A2451) indicates structural changes in the peptidyltransferase center. The possible significance of the chemical protection patterns observed in the Y9C and Y11C mutant ribosomes is discussed below.

DISCUSSION

This study describes the generation and characterization of a new set of *rpl10* yeast alleles based on their ability to promote loss of the Killer phenotype. The mutations predominantly clustered in several regions. Eight mutants

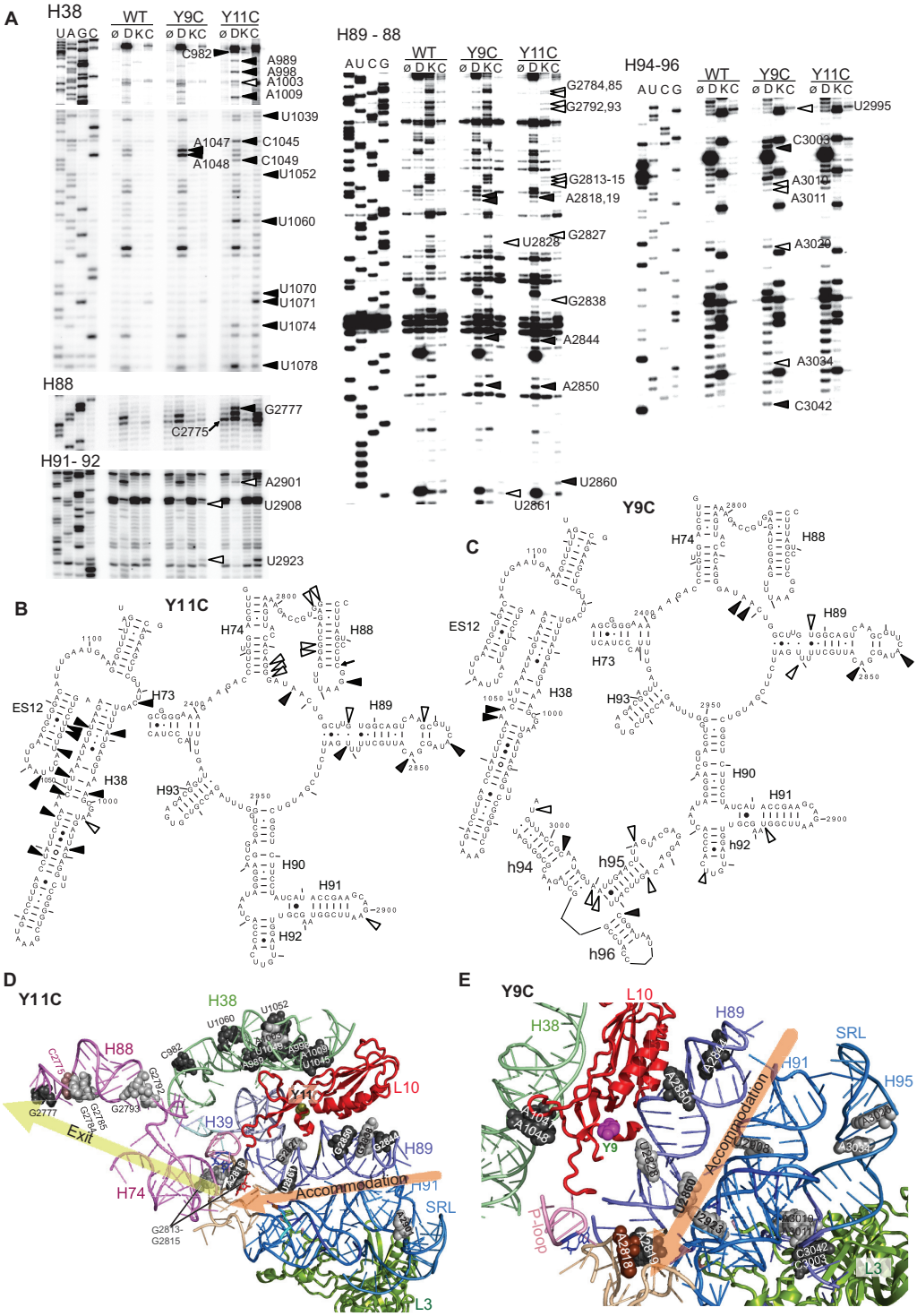

Figure 5. Structure probing of wild-type and mutant ribosomes. (**A**) Autoradiograms of reverse transcriptase primer extension reactions spanning sequences in helix 38 and expansion segment 12, helices 88–92 and helices 94–96. Sequencing reactions (left sides of panels) are labeled corresponding to the rRNA sense strand. Mutants are indicated at top, and bases with altered chemical protection patterns are indicated to the left. Atop each panel lane, ø indicates untreated ribosomes, D is DMS, C denotes CMCT and K stands for kethoxal. Open arrowheads indicate bases that are hyperprotected from chemical attack relative to wild-type, and filled arrowheads denote bases that are more susceptible to chemical attack. The black arrow at C2775 denotes increased in-line cleavage at this site in the Y11C mutant. Yeast 25S rRNA base numbering is used throughout. (**B** and **C**) Localization of bases in yeast 25S rRNA whose modification patterns were affected by the Y11C (B) and Y9C (C) mutants. Protected and deprotected bases are indicated by open and filled arrowheads, respectively, and the arrow at C2775 shows enhanced in-line cleavage. (**D** and **E**) rRNA protection data mapped onto the yeast large subunit crystal structure threaded into that of *H. marismortui* (2). Base numbering follows the *S. cerevisiae* sequence shown in (B) and (C). Hyperprotected bases are colored gray, and deprotected bases are shown in black. In panel E, A2818 (*E. coli* A2451) is colored dark ochre. The path taken by the 3′ end of aa-tRNA as it accommodates into the large subunit is denoted by the orange arrows, while the path it takes out of the peptidyltransferase center is traced by the green arrow in (D).

were identified in the N-terminal 'hook' region composed of residues R7, Y9 and Y11. All these residues either contact the PTC-proximal bulge in the H89 or with nearby residues. The second group, A64, K74, N144, K145 and L152, appear to interact with H89. Group three appears to directly contact or be in close proximity with the bulge in H38 and includes eight mutants at six positions (K15, Y17, V26, Q59, P93 and F94). In particular, K15 and Y17 link Helices 38 and 39, each appearing to make contact with both structures. The fourth group is located in the C-terminal region of L10, the structure of which is currently unresolved. Together with tip of the H38, this region of the protein forms an extension that approaches the L7/L12 stalk. We attribute K40 and G81positions to this group because they topologically represent the base of this extension. Consistent with a previous report (46), no mutations were found in the unstructured loop of L10 that is thought to most closely approach the PTC, thus indirectly suggesting that this loop is either not important for ribosome biogenesis, peptidyltransfer and/or translational fidelity (unlikely), or that it is so important that mutants in this region are inviable (more likely). A full analysis of all of the mutants identified in the current study is beyond the scope of a single manuscript. Thus, we chose to focus more deeply on those located in the N-terminal 'hook' region of L10 in the current study in order to establish a connection with ribosomal protein L3 (see accompanying manuscript by Meskauskas,A. and Dinman,J.D.) with an emphasis on how ribosome structure informs function.

Ribosome structure and elongation factor interactions: an allosteric model

The TC and eEF2 are structural mimics of one another and bind to essentially the same site of the ribosome (1). How then does the ribosome coordinate its interactions with these two ligands at the correct phases of the elongation cycle? The Dontsova group used mutants of Helix 42 in *E. coli* to demonstrate that activation of EF-G may involve allosteric signaling from the peptidyltransferase center to the GAC, and that the difference between the EF-G and TC-binding sites may be due to differences in the positioning of the GAC relative to the SRL (52,53). We subsequently proposed a complementary model suggesting that ribosomal protein L3 functions as the 'gatekeeper to the A-site' within this scheme (9). This model has been expanded and refined in the accompanying manuscript. These studies propose that L3 plays a role in coordinating the orderly binding of the elongation factors and peptidyltransferase activity by participating in a series of local allosteric changes in rRNA structure. Specifically we proposed that the 'open' aa-tRNA accommodation corridor conformation defines the TC-binding site, while the 'closed' conformation favors eEF2 binding. Examination of the atomic scale ribosome structures reveals that L10 lies on the opposite side of the accommodation corridor and PTC from L3 (e.g. see Figure 5D), and data in the accompanying manuscript indicate that bases in H89 that interact with the N-terminal hook of L10 are involved in this process. The data from the current study closely complement those from our studies of L3, in particular with regard to coordination of elongation factor interactions. Specifically, in the Y9C mutant, hyperprotection of the Gate 1 bases (U2860 and U2923, *E. coli* U2492 and U2555), accompanied by increased affinity for eEF2 and decreased affinity for aa-tRNA is consistent with a 'closed' accommodation corridor/eEF2-binding site. Conversely in the Y11C mutant, deprotection of U2861 (*E. coli* U2493) coupled with increased affinity for aa-tRNA and decreased affinity for eEF2 is consistent with the 'open' corridor/TC-binding conformation. In addition, deprotection of G2777 (*E. coli* A2406) and enhanced in-line cleavage of C2775 (*E. coli* U2404) suggests that the 'E-site gate', through which deacylated tRNA passes on its way from the P-site to the E-site and out of the ribosome (39,54–57), is also open in this mutant. The effects of these mutants on ribosome structure along the entire path traversed by tRNAs during the elongation cycle leads us to propose that L10 plays an important role in coordinating tRNA movement through the large subunit.

Anisomycin resistance/hypersensitivity and ribosome structure

The L10 mutants examined in the current study displayed a range of phenotypes related to anisomycin, ranging from strong drug resistance (R7L, R7P and Y9C) to hypersensitive (Y9H, Y9N and Y11C). Anisomycin resistance by ribosomal protein L3 mutants was previously proposed to be due to opening of the accommodation corridor, increasing diffusion rates of the relatively large aa-tRNA into the PTC relative to the much smaller drug (6,9). This model cannot explain the observations made with the L10 mutants in the current study, where Y9C (corridor closed) is drug resistant while Y11C (corridor open) is hypersensitive. Two more-recent studies point to changes in the drug-binding site being responsible for anisomycin resistance (11,58). Mutation of *E. coli* C2452 to U (yeast C2820U, *H. marismortui* 2487U) confers very strong anisomycin resistance. Chemical protection studies in the yeast mutant showed that anisomycin was unable to protect this base from chemical attack, suggesting that anisomycin cannot interact with a U at this position. The X-ray crystal structure of the analogous *H. marismortui* mutant confirmed this model. In the current study, we did not detect any changes in the sensitivity of this base to chemical modifying agents. However the increased sensitivity of the two 5′ adjacent bases (A2818 and A2819, *E. coli* A2450 and A2451) could account for the resistance of the Y9C mutant to this drug. This does not address the question of how Y11C, in which A2818 (*E. coli* A2450) is also deprotected, could be anisomycin hypersensitive. A potential answer might be gleaned from the anisomycin-resistant G2447C and G2447U *H. marismortui* mutants (58). This base contacts anisomycin through a K^+, and the two mutants cause drug resistance by altering the position of this ion. In yeast, the corresponding base is G2815; this base and its two 5′ neighbors are deprotected in the Y11C mutant (Figure 5). We suggest that this mutant may result in a change in this region of the anisomycin-binding pocket that confers increased affinity for anisomycin,

resulting in drug hypersensitivity. This idea is supported by the increased affinity of Y11C for aa-tRNA, the 3′end of which partially overlaps with the anisomycin-binding pocket.

Ribosome structure, translational fidelity and virus maintenance

Some of the L10 'hook' mutants had strong effects on termination codon recognition (Figure 3A). We speculate that this may be explained by open/closed nature of accommodation corridor. The closed conformation, e.g. Y9C, could decrease aa-tRNA accommodation rates, providing more time for ribosomes to reject suppressor tRNAs during the proofreading phase of translation elongation (59). Conversely, the 'open' mutants (Y11C, and perhaps R7L) may inhibit proofreading by allowing faster accommodation of incorrect tRNAs. Since –1 PRF was at best only marginally affected by the mutants examined in the study, it is more likely that the killer virus maintenance defects of the L10 N-terminal 'hook' mutants were due to their strong effects on 60S biogenesis as previously described (44,45).

L10 and information flow through the ribosome

Inspection of Figure 5D shows that L10 lies along a plane formed by Helix 38, Helix 39/L10, Helix 89, Helix 91 and Helix 95. This can be compared to five fingers, with L10 as a proteinaceous prosthesis of Helix 39. In addition, L10 interacts with the D-loop of 5S rRNA (data not shown). Why would nature select for a removable protein to occupy this space rather than simply extending Helix 39? Examination of its placement reveals that L10 is at the center of a topological nexus that interacts with: 5S rRNA, thus connecting it to the B1b and B1c intersubunit bridges at the crown of the large subunit; the GTPase-associated center, connecting it to elongation factor activation; the A-site finger (Helix 38), connecting it with the decoding center through the B1a bridge; and the peptidyltransferase center. We suggest that the information flow through this region of the large subunit is too complex to be monitored by a simple rRNA helix, thus necessitating the evolution of an informationally more complex molecule such as a protein to occupy this site. Thus, we suggest that L10 functions to collect, distribute and coordinate information throughout the large subunit.

The observed effects of the L10 mutants on ribosome structure and function could be explained consequent to 60S mis-assembly defects. This notion is supported by studies of the prokaryotic ortholog L16 showing that it is only important for late assembly steps but that it is not involved in other ribosomal functions (60). However, in support of our model, we note that if mis-assembly were the major issue, then the Y9C and Y11 C mutants would have displayed similar changes in chemical protection patterns. This was not the case. Instead, the chemical protection patterns observed with the Y9C mutants more closely resembled those observed for various mutants of ribosomal protein L3 [(9) and accompanying manuscript], while those for the Y11C mutants more closely resembled those observed for mutants of Helix 38 and of the A-loop (7,11), suggesting that the Y9C and Y11C mutants independently impact on two discrete physical pathways for information flow through the ribosome.

Lastly, is L10 involved in the process of ribosome ratcheting between the pre- and post-translocational states (61)? Comparison of the L10 (bacterial L16, archae L10e) N-terminal regions between seven different high-resolution ribosome structures suggest that it can assume two different conformations: interacting with Helix 89 or with Helix 38 (see Supplementary Figure 2). One possible interpretation of these comparisons is that the hook interacts with Helix 89 when the A-site is unoccupied (the post-translocation state), while it interacts with Helix 38 when the A-site is occupied (pre-translocation state). It is possible that the N-terminal 'hook' of L10 may participate in this process through its interactions with the PTC proximal loop of Helix 89 (post-state) and Helix 38 (pre-state). By this model, interaction of the L10 hook with bases in the PTC-proximal bulge in Helix 89 may help to open the aa-tRNA accommodation corridor. Upon A-site tRNA occupancy, the L10 hook could flip up to interact with H38, releasing the H89 gate base to interact with its partner at the base of Helix 92, which is controlled through the L3 'rocker switch' (see accompanying manuscript by Meskauskas,A. and Dinman,J.D.). By this model then, the Y9C mutant would thermodynamically favor the closed conformation while Y11C would drive it toward the open state. Alternatively, it is possible that no such switch exists, and that the differences in the atomic resolution structures could be due to phylogenetic differences (eukaryotes and archae versus bacteria), or due to different crystallization conditions. The answers to these questions await the availability of high-resolution structures of eukaryotic ribosomes and of bacterial ribosomes complexed with EF-G.

SUPPLEMENTARY DATA

Supplementary Data are available at NAR Online.

ACKNOWLEDGEMENTS

We wish to thank Dr. Arlen Johnson for supplying the *rpl10* gene deletion strain and for plasmids. Thanks to members of the Dinman lab including Rasa Rakauskaite, Jennifer Baxter-Roshek and Johnathan Russ for help and advice. Special thanks to Marat Yusupov for providing deep insights into ribosome structure, and to Jodi Puglisi for his insightful discussions of ribosome dynamics during the 2008 Cold Spring Harbor meeting on Translational Control.

FUNDING

The National Institutes of Health (GM058859 to J.D.D.); the American Heart Association (AHA 0630163N to A.M.); and the Howard Hughes Medical Institute Undergraduate Science Education Program (to S.C.R. through the University of Maryland). Funding for open access charge: NIH GM058859.

Conflict of interest statement. None declared.

REFERENCES

1. Nissen,P., Kjeldgaard,M. and Nyborg,J. (2000) Macromolecular mimicry. *EMBO J.*, **19**, 489–495.
2. Spahn,C.M., Gomez-Lorenzo,M.G., Grassucci,R.A., Jorgensen,R., Andersen,G.R., Beckmann,R., Penczek,P.A., Ballesta,J.P. and Frank,J. (2004) Domain movements of elongation factor eEF2 and the eukaryotic 80S ribosome facilitate tRNA translocation. *EMBO J.*, **23**, 1008–1019.
3. Moazed,D., Robertson,J.M. and Noller,H.F. (1988) Interaction of elongation factors EF-G and EF-Tu with a conserved loop in 23S RNA. *Nature*, **334**, 362–364.
4. Valle,M., Sengupta,J., Swami,N.K., Grassucci,R.A., Burkhardt,N., Nierhaus,K.H., Agrawal,R.K. and Frank,J. (2002) Cryo-EM reveals an active role for aminoacyl-tRNA in the accommodation process. *EMBO J.*, **21**, 3557–3567.
5. Dontsova,O.A. and Dinman,J.D. (2005) 5S rRNA: structure and function from head to toe. *Int. J. Biomed. Sci.*, **1**, 2–7.
6. Meskauskas,A., Petrov,A.N. and Dinman,J.D. (2005) Identification of functionally important amino acids of ribosomal protein L3 by saturation mutagenesis. *Mol. Cell Biol.*, **25**, 10863–10874.
7. Rakauskaite,R. and Dinman,J.D. (2006) An arc of unpaired "hinge bases" facilitates information exchange among functional centers of the ribosome. *Mol. Cell Biol.*, **26**, 8992–9002.
8. Baxter-Roshek,J.L., Petrov,A.N. and Dinman,J.D. (2007) Optimization of ribosome structure and function by rRNA base modification. *PLoS ONE*, **e174**.
9. Meskauskas,A. and Dinman,J.D. (2007) Ribosomal protein L3: gatekeeper to the A-site. *Mol. Cell*, **25**, 877–888.
10. Meskauskas,A., Russ,J.R. and Dinman,J.D. (2008) Structure/function analysis of yeast ribosomal protein L2. *Nucleic Acids Res.*, **36**, 1826–1835.
11. Rakauskaite,R. and Dinman,J.D. (2008) rRNA mutants in the yeast peptidyltransferase center reveal allosteric information networks and mechanisms of drug resistance. *Nucleic Acids Res.*, **36**, 1497–1507.
12. Sanbonmatsu,K.Y., Joseph,S. and Tung,C.S. (2005) Simulating movement of tRNA into the ribosome during decoding. *Proc. Natl Acad. Sci. USA*, **102**, 15854–15859.
13. Schuwirth,B.S., Borovinskaya,M.A., Hau,C.W., Zhang,W., Vila-Sanjurjo,A., Holton,J.M. and Cate,J.H. (2005) Structures of the bacterial ribosome at 3.5 A resolution. *Science*, **310**, 827–834.
14. Selmer,M., Dunham,C.M., Murphy,F.V., Weixlbaumer,A., Petry,S., Kelley,A.C., Weir,J.R. and Ramakrishnan,V. (2006) Structure of the 70S ribosome complexed with mRNA and tRNA. *Science*, **313**, 1935–1942.
15. Korostelev,A., Trakhanov,S., Laurberg,M. and Noller,H.F. (2006) Crystal structure of a 70S ribosome-tRNA complex reveals functional interactions and rearrangements. *Cell*, **126**, 1065–1077.
16. Spahn,C.M., Jan,E., Mulder,A., Grassucci,R.A., Sarnow,P. and Frank,J. (2004) Cryo-EM visualization of a viral internal ribosome entry site bound to human ribosomes: the IRES functions as an RNA-based translation factor. *Cell*, **118**, 465–475.
17. Spahn,C.M., Beckmann,R., Eswar,N., Penczek,P.A., Sali,A., Blobel,G. and Frank,J. (2001) Structure of the 80S ribosome from Saccharomyces cerevisiae–tRNA-ribosome and subunit-subunit interactions. *Cell*, **107**, 373–386.
18. Giaever,G., Chu,A.M., Ni,L., Connelly,C., Riles,L., Veronneau,S., Dow,S., Lucau-Danila,A., Anderson,K., Andre,B. *et al.* (2002) Functional profiling of the Saccharomyces cerevisiae genome. *Nature*, **418**, 387–391.
19. Johnson,A.W., Lund,E. and Dahlberg,J. (2002) Nuclear export of ribosomal subunits. *Trends Biochem. Sci.*, **27**, 580–585.
20. Dick,F.A. and Trumpower,B.L. (1998) Heterologous complementation reveals that mutant alleles of QSR1 render 60S ribosomal subunits unstable and translationally inactive. *Nucleic Acids Res.*, **26**, 2442–2448.
21. Eisinger,D.P., Dick,F.A. and Trumpower,B.L. (1997) Qsr1p, a 60S ribosomal subunit protein, is required for joining of 40S and 60S subunits. *Mol. Cell Biol.*, **17**, 5136–5145.
22. Zuk,D., Belk,J.P. and Jacobson,A. (1999) Temperature-sensitive mutations in the Saccharomyces cerevisiae MRT4, GRC5, SLA2 and THS1 genes result in defects in mRNA turnover. *Genetics*, **153**, 35–47.
23. Wickner,R.B. (1996) Prions and RNA viruses of *Saccharomyces cerevisiae*. *Annu. Rev. Genet.*, **30**, 109–139.
24. Inoue,H., Nojima,H. and Okayama,H. (1990) High efficiency transformation of Escherichia coli with plasmids. *Gene*, **96**, 23–28.
25. Dinman,J.D. and Kinzy,T.G. (1997) Translational misreading: mutations in translation elongation factor 1α differentially affect programmed ribosomal frameshifting and drug sensitivity. *RNA*, **3**, 870–881.
26. Ito,H., Fukuda,Y., Murata,K. and Kimura,A. (1983) Transformation of intact yeast cells treated with alkali cations. *J. Bacteriol.*, **153**, 163–168.
27. Dinman,J.D. and Wickner,R.B. (1994) Translational maintenance of frame: mutants of *Saccharomyces cerevisiae* with altered -1 ribosomal frameshifting efficiencies. *Genetics*, **136**, 75–86.
28. Harger,J.W. and Dinman,J.D. (2003) An *in vivo* dual-luciferase assay system for studying translational recoding in the yeast *Saccharomyces cerevisiae*. *RNA*, **9**, 1019–1024.
29. Jacobs,J.L. and Dinman,J.D. (2004) Systematic analysis of bicistronic reporter assay data. *Nucleic Acids Res.*, **32**, e160–e170.
30. Meskauskas,A. and Dinman,J.D. (2001) Ribosomal protein L5 helps anchor peptidyl-tRNA to the P-site in Saccharomyces cerevisiae. *RNA*, **7**, 1084–1096.
31. Muhlrad,D., Hunter,R. and Parker,R. (1992) A rapid method for localized mutagenesis of yeast genes. *Yeast*, **8**, 79–82.
32. Sikorski,R.S. and Hieter,P. (1989) A system of shuttle vectors and yeast host strains designed for efficient manipulation of DNA in *Saccharomyces cerevisiae*. *Genetics*, **122**, 19–27.
33. Boeke,J.D., LaCroute,F. and Fink,G.R. (1984) A positive selection for mutants lacking orotidine-5′-phosphate decarboxylase activity in yeast: 5-fluoro-orotic acid resistance. *Mol. Gen. Genet.*, **197**, 345–346.
34. Dinman,J.D. and Wickner,R.B. (1992) Ribosomal frameshifting efficiency and Gag/Gag-pol ratio are critical for yeast M_1 double-stranded RNA virus propagation. *J. Virol.*, **66**, 3669–3676.
35. Cui,Y., Kinzy,T.G., Dinman,J.D. and Peltz,S.W. (1998) Mutations in the *MOF2/SUI1* gene affect both translation and nonsense-mediated mRNA decay. *RNA*, **5**, 794–804.
36. Plant,E.P., Wang,P., Jacobs,J.L. and Dinman,J.D. (2004) A programmed -1 ribosomal frameshift signal can function as a cis-acting mRNA destabilizing element. *Nucleic Acids Res.*, **32**, 784–790.
37. Sachs,A.B. and Davis,R.W. (1989) The poly(A) binding protein is required for poly(A) shortening and 60S ribosomal subunit-dependent translation initiation. *Cell*, **58**, 857–867.
38. Ban,N., Nissen,P., Hansen,J., Moore,P.B. and Steitz,T.A. (2000) The complete atomic structure of the large ribosomal subunit at 2.4 A resolution. *Science*, **289**, 905–920.
39. Jenner,L., Rees,B., Yusupov,M. and Yusupova,G. (2007) Messenger RNA conformations in the ribosomal E site revealed by X-ray crystallography. *EMBO Rep.*, **8**, 846–850.
40. Harms,J.M., Wilson,D.N., Schluenzen,F., Connell,S.R., Stachelhaus,T., Zaborowska,Z., Spahn,C.M. and Fucini,P. (2008) Translational regulation via L11: molecular switches on the ribosome turned on and off by thiostrepton and micrococcin. *Mol. Cell*, **30**, 26–38.
41. Wickner,R.B. (1991) Yeast RNA virology: the killer systems. In Broach,J.R., Jones,E.W. and Pringle,J.R. (eds), *The Molecular and Cellular Biology of the Yeast Saccharomyces: Genome Dynamics, Proteins Synthesis, and Energetics*, Vol. 1. Cold Spring Harbor Press, Cold Spring Harbor, NY, pp. 263–296.
42. Icho,T. and Wickner,R.B. (1989) The double-stranded RNA genome of yeast virus L-A encodes its own putative RNA polymerase by fusing two open reading frames. *J. Biol. Chem.*, **264**, 6716–6723.
43. Dinman,J.D., Icho,T. and Wickner,R.B. (1991) A -1 ribosomal frameshift in a double-stranded RNA virus forms a Gag-pol fusion protein. *Proc. Natl Acad. Sci. USA*, **88**, 174–178.
44. Ohtake,Y. and Wickner,R.B. (1995) Yeast virus propagation depends critically on free 60S ribosomal subunit concentration. *Mol. Cell Biol.*, **15**, 2772–2781.
45. Carroll,K. and Wickner,R.B. (1995) Translation and M_1 dsRNA propagation: *MAK18 = RPL41B* and cycloheximide curing. *J. Bacteriol.*, **177**, 2887–2891.

46. Hofer,A., Bussiere,C. and Johnson,A.W. (2007) Mutational analysis of the ribosomal protein RPL10 from yeast. *J. Biol. Chem.*, **282**, 32630–32639.
47. Hansen,J.L., Moore,P.B. and Steitz,T.A. (2003) Structures of five antibiotics bound at the peptidyl transferase center of the large ribosomal subunit. *J. Mol. Biol.*, **330**, 1061–1075.
48. Carter,A.P., Clemons,W.M., Brodersen,D.E., Morgan-Warren,R.J., Wimberly,B.T. and Ramakrishnan,V. (2000) Functional insights from the structure of the 30S ribosomal subunit and its interactions with antibiotics. *Nature*, **407**, 340–348.
49. Bidou,L., Stahl,G., Hatin,I., Namy,O., Rousset,J.P. and Farabaugh,P.J. (2000) Nonsense-mediated decay mutants do not affect programmed -1 frameshifting. *RNA*, **6**, 952–961.
50. Johnson,A.W., Ho,J.H., Kallstrom,G., Trotta,C., Lund,E., Kahan,L., Dahlberg,J. and Hedges,J. (2001) Nuclear export of the large ribosomal subunit. *Cold Spring Harb. Symp. Quant. Biol.*, **66**, 599–605.
51. Inoue,T., Sullivan,F.X. and Cech,T.R. (1985) Intermolecular exon ligation of the rRNA precursor of Tetrahymena: oligonucleotides can function as 5′ exons. *Cell*, **43**, 431–437.
52. Sergiev,P.V., Lesnyak,D.V., Burakovsky,D.E., Kiparisov,S.V., Leonov,A.A., Bogdanov,A.A., Brimacombe,R. and Dontsova,O.A. (2005) Alteration in location of a conserved GTPase-associated center of the ribosome induced by mutagenesis influences the structure of peptidyltransferase center and activity of elongation factor G. *J. Biol. Chem.*, **280**, 31882–31889.
53. Sergiev,P.V., Bogdanov,A.A. and Dontsova,O.A. (2005) How can elongation factors EF-G and EF-Tu discriminate the functional state of the ribosome using the same binding site? *FEBS Lett.*, **579**, 5439–5442.
54. Agrawal,R.K., Heagle,A.B., Penczek,P., Grassucci,R.A. and Frank,J. (1999) EF-G-dependent GTP hydrolysis induces translocation accompanied by large conformational changes in the 70S ribosome. *Nat. Struct. Biol.*, **6**, 643–647.
55. Harms,J., Schluenzen,F., Zarivach,R., Bashan,A., Gat,S., Agmon,I., Bartels,H., Franceschi,F. and Yonath,A. (2001) High resolution structure of the large ribosomal subunit from a mesophilic eubacterium. *Cell*, **107**, 679–688.
56. Valle,M., Zavialov,A., Sengupta,J., Rawat,U., Ehrenberg,M. and Frank,J. (2003) Locking and unlocking of ribosomal motions. *Cell*, **114**, 123–134.
57. Gao,H., Sengupta,J., Valle,M., Korostelev,A., Eswar,N., Stagg,S.M., Van Roey,P., Agrawal,R.K., Harvey,S.C., Sali,A. *et al.* (2003) Study of the structural dynamics of the E. coli 70S ribosome using real-space refinement. *Cell*, **113**, 789–801.
58. Blaha,G., Gurel,G., Schroeder,S.J., Moore,P.B. and Steitz,T.A. (2008) Mutations outside the anisomycin-binding site can make ribosomes drug-resistant. *J. Mol. Biol.*, **379**, 505–519.
59. Rodnina,M.V. and Wintermeyer,W. (2001) Fidelity of aminoacyl-tRNA selection on the ribosome: kinetic and structural mechanisms. *Annu. Rev. Biochem.*, **70**, 415–435.
60. Franceschi,F.J. and Nierhaus,K.H. (1990) Ribosomal proteins L15 and L16 are mere late assembly proteins of the large ribosomal subunit. Analysis of an Escherichia coli mutant lacking L15. *J. Biol Chem.*, **265**, 16676–16682.
61. Frank,J. and Agrawal,R.K. (2000) A ratchet-like inter-subunit reorganization of the ribosome during translocation. *Nature*, **406**, 318–322.
62. Cui,Y., Dinman,J.D. and Peltz,S.W. (1996) *mof4-1* is an allele of the *UPF1/IFS2* gene which affects both mRNA turnover and -1 ribosomal frameshifting efficiency. *EMBO J.*, **15**, 5726–5736.
63. Ohtake,Y. and Wickner,R.B. (1995) KRB1, a suppressor of mak7-1 (a mutant RPL4A), is RPL4B, a second ribosomal protein L4 gene, on a fragment of Saccharomyces chromosome XII. *Genetics*, **140**, 129–137.